Electron Momentum Densities by $(\gamma, e \gamma)$ -Spectroscopy *

F. Bell**, Th. Tschentscher⁺, J. R. Schneider⁺, and A. J. Rollason⁺ + Hamburger Synchrotronstrahlungslabor HASYLAB at DESY, Notkestr. 85, D-2000 Hamburg 52, Germany

Z. Naturforsch. 48a, 273-278 (1993); received October 8, 1991

We report coincidence measurements of inelastically scattered 148 keV photons and the recoil electrons generated within thin Al and Cu foils. We have analyzed both the Doppler broadening of the scattered photon intensity and the angular correlation of the recoil electron. This corresponds to different scans through the three-dimensional electron momentum density of the target. Estimates of the triple-differential cross-section for Compton scattering are given. The experiment was performed with synchrotron radiation from a bending magnet of the DORIS storage ring at DESY, Hamburg.

Key words: Electron momentum densities; Compton scattering; Synchrotron radiation.

1. Introduction

In the past, deep inelastic photon scattering - i.e. Compton scattering - has been used to investigate so-called Compton profiles of valence electrons in solids [1, 2]. The momentum distribution of the electrons causes a Doppler broadening of the scattered radiation. If the recoil electron is not observed, the double-differential cross-section is proportional to the Compton profile, which is obtained by integration of the electron momentum density (EMD) over the momentum components perpendicular to the photon momentum transfer vector. However, if the electron is detected in coincidence with the scattered photon, the triple-differential cross-section is proportional to the EMD itself. It is our final aim to extract information about the EMD from such measurements. Recently, we have demonstrated the feasibility of such a $(\gamma, e \gamma)$ experiment [3-5]. The idea of fixing the kinematics by a coincidence condition is the same as in positron annihilation experiments or in (e, 2e) spectroscopy, which means that the information one gains from all three experimental techniques is similar or even iden-

* Presented at the Sagamore X Conference on Charge, Spin and Momentum Densities, Konstanz, Fed. Rep. of Germany, September 1-7, 1991.

** Sektion Physik, Universität München, Am Coulombwall 1, D-W-8046 Garching, Fed. Rep. of Germany.

++ Department of Physics, University of Keele, Staffordshire, ST5 5BG, England.

Reprint requests to Prof. Dr. J. R. Schneider, Hamburger Synchrotronstrahlungslabor HASYLAB at DESY, Notkestr. 85, D-W-2000 Hamburg 52, Fed. Rep. of Germany.

tical. This holds especially for $(\gamma, e \gamma)$ and (e, 2 e) reactions. In both cases the triple-differential cross-section is proportional to the EMD, the proportionality factor being, roughly speaking, the Klein-Nishina or the Rutherford cross-section.

If either (e, 2e) or $(\gamma, e\gamma)$ reactions are applied to solid-state targets, both suffer from strong incoherent elastic scattering of the electrons. This smearing of the electron direction disturbs to some extent the evaluation of the EMD. This is probably the reason why there have been only a few groups who applied (e, 2e) reactions to solids [6-12]. Although this effect exists in our case also, it is less important than for (e, 2e) spectroscopy, since one of the collision partners is a photon restricting the multiple scattering to the outgoing recoil electron.

The first $(\gamma, e \gamma)$ experiments is due to Bothe and Geiger [13]. Of course, the aim of this experiment – and that of later investigations, which are reviewed in the article of Evans [14] – was not the evaluation of the momentum density, but the demonstration of the strict validity of energy and momentum conservation in individual photon–electron encounters.

2. Cross-Section and Kinematics

In this chapter we will shortly discuss the triple-differential cross-section and the relevant scattering kinematics. Suppose a photon with four-vector $(k, i\omega)$ is scattered at an electron with (p, iE), resulting in a scattered photon with $(k', i\omega')$ and a recoil electron with (p', iE'). One then obtains within the relativistic impulse approximation for the four-fold differential

Hamburger Synchrotronstrahlungslabor HASYLAB at Deutsches Elektronen-Synchrotron DESY, Notkestr. 85, D-W-2000 Hamburg 52, Fed. Rep. of Germany.

cross-section for deep inelastic photon scattering [15]

$$\begin{split} \frac{\mathrm{d}^4 \sigma}{\mathrm{d}\omega' \, \mathrm{d}E' \, \mathrm{d}\Omega_{\gamma} \, \mathrm{d}\Omega_{\mathrm{e}}} \\ &= \frac{\alpha^2}{2} \frac{\omega'}{\omega} \sum_{i} \frac{p'}{E} \varrho_i(\mathbf{p}) X_{\mathrm{ph}} \, \delta(\omega + E - \omega' - E') \end{split} \tag{1}$$

(we use natural units, i.e. $\hbar = m = c = 1$; then $e^2 = \alpha$ holds, where α is the fine structure constant). Within the independent-electron model and the frozenorbital approximation, ϱ_i is the EMD of the singleparticle state i. Momentum conservation demands p = k' + p' - k. The scattering function X_{ph} depends only weakly on the electron momentum p, and the initial electron energy $E = 1 - E_{\rm B}^{i}$ is determined by the binding energy $E_{\rm B}^i$. In the following we will neglect the influence of the binding energies, since the cross-section of (1) is dominated by contributions from the valence electrons with binding energies less than 200 eV. This holds for targets such as Al and Cu. Since the energy resolution of the photon detector is 0.5 keV only, shifts owing to the binding energy $E_{\rm B}^i$ cannot be detected. Thus we obtain from (1)

$$\frac{\mathrm{d}^{3}\sigma}{\mathrm{d}\omega'\,\mathrm{d}\Omega_{\gamma}\,\mathrm{d}\Omega_{e}} = \frac{\alpha^{2}}{2}\frac{\omega'}{\omega}p'X_{\mathrm{ph}}\,\varrho\left(\boldsymbol{p}\right),\tag{2}$$

where $\varrho = \sum \varrho_i$ is the total EMD and the cross-section function reads

$$X_{\rm ph} = \frac{\omega'}{\omega} + \frac{\omega}{\omega'} - (1 - P)\sin^2\Theta; \tag{3}$$

here the Stokes parameter P describes the degree of linear photon polarisation [16]. In (3) we have neglected a weak p-dependence [15, 17]. Θ is the photon scattering angle. Scans through the EMD can be made in two different ways:

1) For fixed scattering angles one measures either the Doppler broadening $\Delta\omega'$ in the photon detector or $\Delta E'$ in the electron detector (owing to energy conservation one has $\Delta\omega'=-\Delta E'$). This broadening results from intrinsic electron momentum components p_{\parallel} parallel to the momentum transfer vector $\pmb{K}=\pmb{k}-\pmb{k}'$. For high-energy photons one obtains

$$p_{\parallel} = \frac{\omega}{K \, \omega_0'} \Delta \omega'. \tag{4}$$

Here

$$\omega_0' = \frac{\omega}{1 + \omega(1 - \cos \Theta)} \tag{5}$$

is the scattered-photon energy for $\mathbf{p} = 0$ and $\Delta \omega' = \omega' - \omega'_0$.

2) For fixed energies one measures the angular correlation between the scattered photon (scattering angle Θ) and the recoil electron (scattering angle Φ). For an electron initially at rest (i.e. p = 0) the recoil electron appears at an angle Φ_0 :

$$\operatorname{ctg}\Phi_{0} = (1+\omega)\operatorname{tg}(\Theta/2). \tag{6}$$

If the electron has initially a momentum component p_{\perp} perpendicular to K, then

$$p_{\perp} = K \, \Delta \Phi \tag{7}$$

with $\Delta \Phi = \Phi_0 - \Phi$.

Thus, by measuring the coincidence count rate as a function either of $\Delta\omega'$ or of $\Delta\Phi$, scans through the EMD can be made for momentum components either parallel or perpendicular to the momentum transfer vector \mathbf{K} : $\varrho = \varrho \left[(p_{\parallel}^{2} + p_{\perp}^{2})^{1/2} \right]$.

3. Experiment

The experiments were performed using synchrotron radiation from a bending magnet of DORIS II at DESY, Hamburg, with a critical energy of 27 keV. The photon beam was monochromated by a Ge crystal in (220) transmission geometry. The energy width of the beam was about 1 keV at $\omega = 148$ keV. The photon detector - an intrinsic Ge diode with a resolution of 0.5 keV (FWHM) – was placed at $\Theta = 140^{\circ}$ and the electron detector – an implanted planar Si-diode with a resolution of about 7 keV (FWHM) - could be moved through an angular range $\Delta \Phi = \pm 10^{\circ}$ around $\Phi_0 = 15.8^{\circ}$. Both detectors were coplanar (Figure 1). The solid angles of the detectors were $\Delta\Omega_{\gamma} = 0.4 \text{ msr}$ and $\Delta\Omega_e = 0.3$ msr. The targets were thin self-supporting Al and Cu foils. The storage ring was operated in the single-bunch mode with a bunch length $\tau_L = 0.15$ ns and a bunch distance $\tau_B = 960$ ns. τ_L is small and $\tau_{\rm B}$ is large compared to the time resolution of our coincidence circuit (~ 120 ns), which means that true coincidences are events that occur during the same bunch. Concerning accidental coincidences there is a remarkable difference if compared to dc-machines. The continuous distribution of uncorrelated events obtained with the latter ones is compressed into bunches in an ac-machine, by which their contribution is enhanced by a factor $1/\eta$, where $\eta = \tau_L/\tau_B$ is the duty cycle of the storage ring. Owing to the very

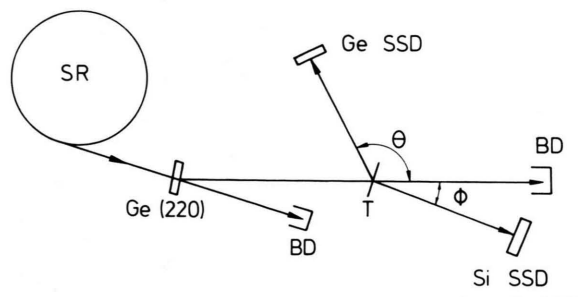


Fig. 1. The experimental setup. SR: storage ring, Ge (220): monochromator, BD: beam dump, Ge SSD: photon detector, Si SDD: electron detector, T: target.

poor duty cycle of DORIS II in the single-bunch mode, this enhancement is large in our case ($\sim 6 \cdot 10^3$). Thus we obtain for the accidental count rate n_a

$$n_{\rm a} = n_1 \, n_2 \, \tau_{\rm L} / \eta = n_1 \, n_2 \, \tau_{\rm B}, \tag{8}$$

where the n_i are the macroscopic count rates of the photon and electron detector [18]. Equation (8) means that the contribution of uncorrelated events is independent of the time resolution of the coincidence circuit, which can be as high as a few ns (e.g. in (e, 2 e) experiments). Nevertheless, a time spectrum 4 μ s wide showed no accidental counts due to uncorrelated events from neighbouring bunches. This is due to very low single count rates n_i , which result from the small Klein-Nishina cross-section and the thin target foils.

Experimental quantities like the divergence of the primary photon beam, its energy band width, the solid angles and the energy resolution of both detectors and, last not least, the finite extension of the beam spot at the target determine a three-dimensional resolution volume in momentum space that is approximately a cube with an edge length of about 0.7 au.

4. Experimental Results

Figure 2 is an example for an angular correlation experiment. The target was a 20 μ m thin Al foil. For the experimental situation mentioned above the momentum transfer vector is about K=62 au. Figure 2 shows the coincidence count rate as a function of $\Delta \Phi = \Phi - \Phi_0$. In order to improve statistics we have summed in this particular case at each angular setting over the energy distribution of the scattered photons, i.e. over the p_{\parallel} -components of the EMD. The shape of the angular distribution is mainly determined by valence electrons with a momentum range given by the

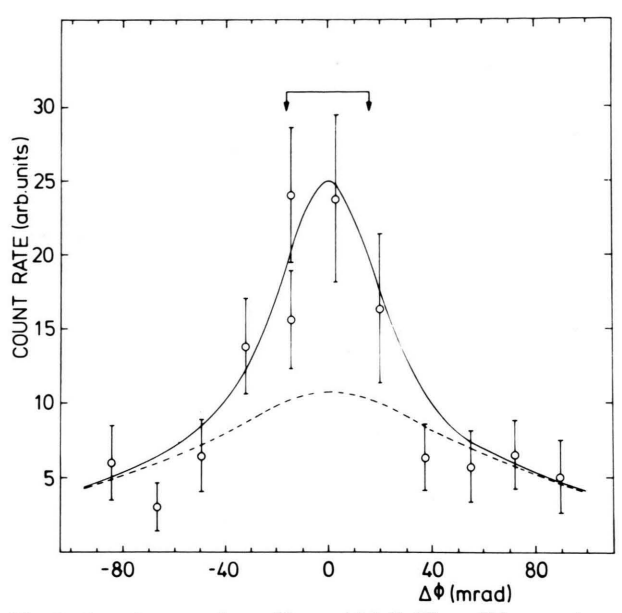


Fig. 2. Angular scan for a 20 µm Al foil. The solid curve is the theoretical expectation and the dashed curve is the background owing to multiply scattered electrons. The arrows indicate the range of the valence electrons.

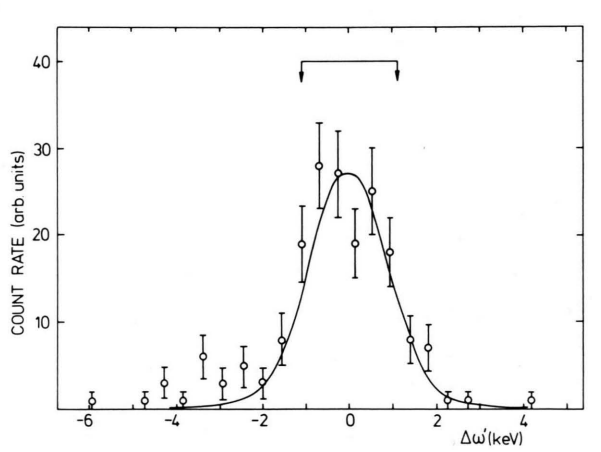


Fig. 3. Doppler-broadened coincident-photon spectrum for a 120 nm Al foil. The solid curve is the theoretical expectation. The arrows indicate the range of the valence electrons.

Fermi momentum $p_{\rm F}=0.94$ au [19]. The corresponding width $\Delta\Phi$ (FWHM) = $2\,p_{\rm F}/K$ (see (7)) amounts to 31 mrad and is indicated by arrows in Figure 2. The recoil electrons have an energy of about 50 keV and a mean free path for elastic scattering of about 50 nm, which means that especially the tails of the momentum distribution in Fig. 2 are strongly influenced by multiple scattering. The amount of multiply scattered

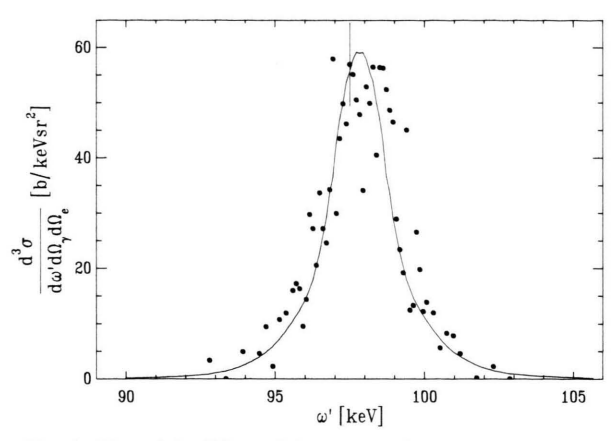


Fig. 4. The triple-differential cross-section as a function of the scattered-photon energy. The target was a 80 nm Cu foil. The solid curve represents the theoretical cross-section of (2).

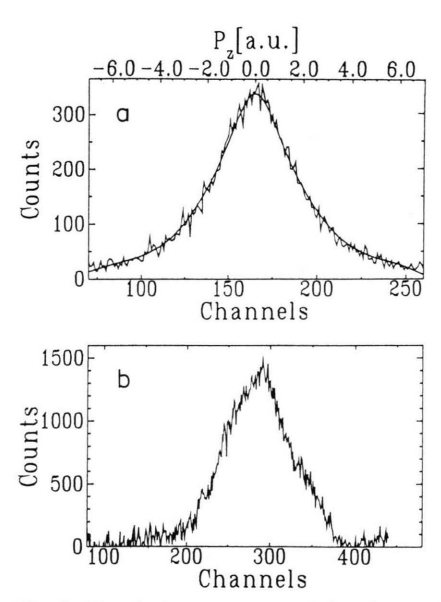


Fig. 5. The singles count rate of the photon detector (Fig. 5a) and the electron detector (Fig. 5b) obtained simultaneously. The solid curve in Fig. 5a is the Compton profile of Cu obtained by Paakkari et al. [24].

electrons has been calculated by a Monte-Carlo procedure [20] and is indicated by the broken curve in Figure 2. The peak on top is due to unscattered electrons created within the last few mean free paths for elastic scattering.

Figure 3 shows the Doppler broadening of the scattered-photon intensity for fixed scattering angles ($\Theta=140^{\circ}$, $\Phi=16^{\circ}$). The target was a 120 nm thin Al foild. The solid curve represents the theoretical EMD of Al convoluted with the energy resolution of the

photon detector. Again, if it is assumed that the EMD is dominated by the valence electrons, the width of the curve in Fig. 3 is given by $\Delta\omega' = 2 K \omega_0' p_F/\omega = 2.2 \text{ keV}$ (see (4)). This width is indicated by arrows. Although the data of Figs. 2 and 3 are count rates and the comparison with theoretical EMDs holds on a relative scale only, we have also tried to evaluate the triple-differential cross-section. Fig. 4 shows this for a photon scattering angle $\Theta = 140^{\circ}$ and an electron emission angle $\Phi = 16^{\circ}$ obtained by an 80 nm thin copper foil. In essence, the experimental data points have been converted into a cross-section by comparing the photon singles count rate with the well-known double-differential cross-section [21, 22]. The solid curve represents the cross-section of (2). The EMD $\varrho(p)$ was taken from the calculation of Bross [23] who used the modified augmented plane-wave method to calculate the sperically averaged EMD of Cu including the $(3 s)^2$ and $(3 p)^6$ states into the band structure. Deeper lying states do not contribute significantly to $\varrho(p)$ within the momentum range that corresponds to the scattered photon energies of Figure 4. For the calculation of (3) it was assumed that the synchrotron radiation was 90% linearly polarized with a polarization vector lying in the scattering plane (which means P = -0.9). The solid curve in Fig. 4 has been fitted to the experimental data by multiplying the theory with the constant factor of 0.8. Since we estimate a systematic error of about 40% owing to errors in the determination of detector efficiencies and solid angles, the cross-section of (2) reproduces the experimental results. Figure 5 shows the singles count rates of the photon detector (Fig. 5a) and electron detector (Fig. 5b) that belong to the triple-differential cross-section of Figure 4. These count rates are proportional to the Compton profiles of the photon and electron branch, respectively. In Fig. 5 a the solid curve represents the Compton profile of Paakkari et al. [24] obtained by a Cu target that was approximately 10⁴ times thicker than our foil. This profile has been convoluted by our energy resolution and fitted by a common factor to the experimental data. We have abandoned to apply the same procedure to the electron branch, since the width of the count rate curve in Fig. 5b is dominated by the poor energy resolution of the electron detector rather than by the momentum distribution of the electrons. Inspection of the total count rates in Fig. 5a and b reveals that far more electrons are ejected into the electron detector than photons into the photon detector, though the solid angles and efficiencies are roughly the

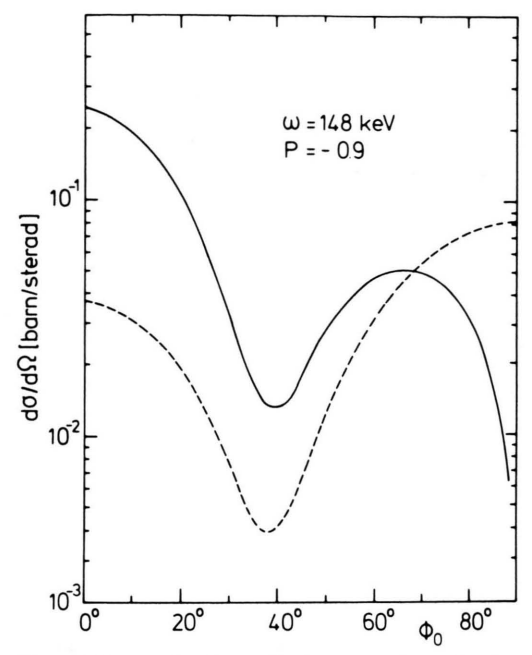


Fig. 6. The single-differential cross-sections for the photon branch (broken curve) and for the electron branch (solid curve). The cross-sections hold for a photon energy $\omega = 148 \text{ keV}$ and a Stokes parameter P = -0.9.

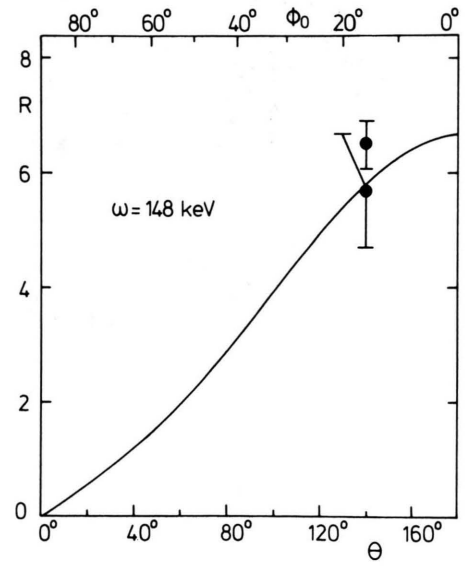


Fig. 7. The cross-section ratio R as a function of the photon scattering angle Θ and the electron ejection angle Φ_0 .

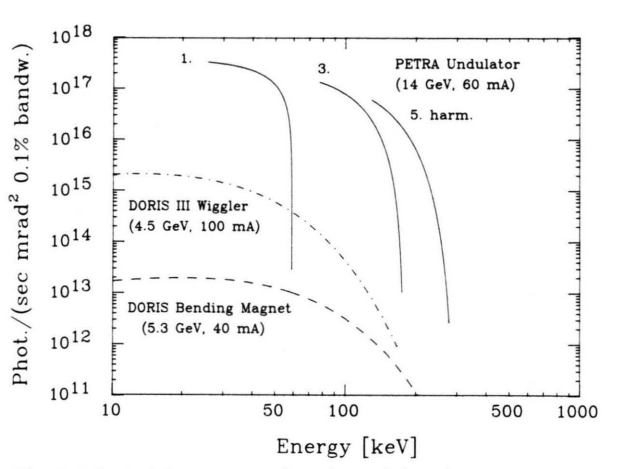


Fig. 8. The brightness as a function of the photon energy.

same. The reason behind is that the single-differential cross-sections $d\sigma/d\Omega_{\gamma}$ and $d\sigma/d\Omega_{\rm e}$ are quite different. Figure 6 shows the cross-sections for scattering a photon by an angle Θ and for ejecting an electron at an angle Φ_0 where both angles are connected via (6). It is clearly seen that the electron cross-section is by far larger, especially for small ejection angles. From (6) one obtains for the cross-section ratio

$$R = \frac{\mathrm{d}\sigma/\mathrm{d}\Omega_{\mathrm{e}}}{\mathrm{d}\sigma/\mathrm{d}\Omega_{\gamma}}$$

$$= \frac{4}{1+\omega} [1+\omega(2+\omega)\sin^2(\Theta/2)]^{3/2} \sin(\Theta/2). \quad (9)$$

Figure 7 shows the cross-section ratio R as a function of Θ and Φ_0 . Clearly, the experimental points reproduce the theoretical ratio of (9) (solid curve). Figures 4 and 7 represent tests of the triple-differential cross-section and of the single-differential cross-section for the electron branch, which, to our knowledge, have not been done before.

5. Conclusions

We believe that the data shown demonstrate the feasibility of a $(\gamma, e \gamma)$ experiment and that EMDs can be extracted. We have verified that deep inelastic photon scattering can be described by the relativistic impulse approximation of (2). Although we have used the most intensive γ -ray source that is available – synchrotron radiation from a lepton storage ring – the data still suffer from rather bad statistics. The data of Fig. 4

have been accumulated in 33 hours of beam time with an intensity of $2 \cdot 10^9$ photons/s at the target. If one would try to obtain such a collimated beam intensity from a radioactive source, the remarkable y-activity of about 10¹⁶ Bq would be required.

Since we are working at a centre of high-energy physics (DESY), it is obvious to look for an alternative to the DORIS ring. Figure 8 shows a calculation of the brightness for an undulator at the 14 GeV PETRA machine [25]. For comparison, the brightness of a bending magnet at DORIS II - this corresponds to the situation of the experimental data shown in this paper – and a wiggler at DORIS III – the near future - are also shown. The fifth harmonic of such an undulator would increase the brightness at $\omega = 150 \text{ keV}$ by more than 4 orders of magnitude compared to DORIS II or III. Because the solid angle accepted by

the $(\gamma, e \gamma)$ experiment performed at a DORIS II bending magnet is larger than the solid angle the PETRA undulator would provide, the effective gain factor is between 10³ and 10⁴. At the same time the PETRA bunch distance $\tau_B = 100 \text{ ns}$ is about a factor of 10 smaller than in DORIS II and allows therefore much higher singles count rates n_i (see (8)). It is therefore expected that the strong increase in intensity can effectively be used. Consequently, there is no doubt that this would increase our accuracy considerably.

6. Acknowledgement

The authors are grateful to Th. Kracht of HASY-LAB, who developed the software for the data acquisition system.

- [1] M. J. Cooper, Rep. Prog. Phys. 48, 415 (1985).
- [2] B. Williams (ed.), Compton Scattering, McGraw-Hill, New York 1977.
- [3] A. J. Rollason, F. Bell, and J. R. Schneider, Nucl. Instr. Meth. A 281, 147 (1989).
- [4] A. J. Rollason, F. Bell, J. R. Schneider, and W. Drube, Solid State Commun. **72**, 297 (1989). [5] F. Bell, A. J. Rollason, J. R. Schneider, and W. Drube,
- Phys. Rev. B 41, 4887 (1990).
- [6] R. Camilloni, A. Giardini Guidoni, R. Tiribelli, and G. Stefani, Phys. Rev. Lett. 29, 618 (1972).
- [7] N. M. Persiantseva, N. A. Krasilnikova, and V. G. Neudachin, [Sov. Phys. JETP 49, 530 (1979)], Zh. Eksp. Teor. Fiz. 76, 1047 (1979).
- [8] C. Gao, A. L. Ritter, J. R. Dennison, and N. A. Holzwarth, Phys. Rev. B 37, 3914 (1988).
- [9] C. Gao, Y. Y. Wang, A. L. Ritter, and J. R. Dennison, Phys. Rev. Lett. 62, 945 (1989).
- [10] P. Hayes, J. F. Williams, and J. Flexman, Phys. Rev. B 43, 1928 (1991).
- [11] P. Hayes, M. A. Bennett, J. Flexman, and J. F. Williams, Phys. Rev. B 38, 13371 (1988).
- [12] J. Lower, S. M. Bharathi, Yu Chen, K. J. Nygaard, and E. Weigold, 1990, preprint, The Flinders University of South Australia.

- [13] W. Bothe and H. Geiger, Z. Phys. 32, 639 (1925).
- [14] R. D. Evans, Handbuch der Physik, ed. S. Flügge, Vol. XXXIV, Springer, Berlin, 1958.
- R. Ribberfors, Phys. Rev. B 12, 3136 (1975).
- [16] F. W. Lipps and H. A. Tolhoek, Physica 20, 395 (1954).
- [17] P. Holm, Phys. Rev. A 37, 3706 (1988).
- [18] K. Hämäläinen, Nucl. Instrum. Meth. A 297, 521 (1990).
 [19] N. Shiotani, N. Sakai, M. Ito, O. Mao, F. Itoh, H. Kawata, Y. Amemiya, and M. Ando, J. Phys.: Condens.
- Matter 1, SA 27 (1989). F. Bell, Th. Tschentscher, J. R. Schneider, and A. J. Rollason, J. Phys.: Condens. Matter 3, 5587 (1991).
- [21] A. Reineking, R. Wenskus, A. Baumann, D. Schaupp, P. Rullhusen, F. Smend, and M. Schumacher, Phys. Lett. **95 A**, 29 (1983).
- [22] R. Wenskus, A. Baumann, P. Rullhusen, D. Schaupp, F. Smend, and M. Schumacher, Z. Phys. A 320, 179 (1985).
- H. Bross, J. Phys. F 12, 2249 (1982).
- [24] T. Paakkari, S. Manninen, and K. F. Berggren, Phys. Fenn. 10, 207 (1975).
- [25] W. Brefeld and P. Gürtler, Proc. of IEEE, Particle Accelerator Conference, Stanford 1991.